Experimental and Computational Study of the Electronic Structural Changes in $LiTi_2O_4$ Spinel Compounds upon Electrochemical Li Insertion Reactions

Wonkyung Ra, Masanobu Nakayama, Yoshiharu Uchimoto, and Masataka Wakihara*

Department of Applied Chemistry, Graduate School of Science and Engineering, Tokyo Institute of Technology, Ookayama 2-12-1, Meguro-ku, Tokyo 152-8552, Japan

Received: July 20, 2004

Electronic structural changes in $LiTi_2O_4$ spinel compounds upon electrochemical lithium insertions were investigated by X-ray absorption spectroscopy (XAS) measurements and first principles calculations based on spin-polarized density functional theory. Ti K-edge, O K-edge XAS spectra and theoretical calculations indicate that oxide ions as well as titanium ions are involved in electronic structural changes caused by electrochemical lithium ion insertions. The considerable effect of the oxide ions in the early 3d transition metal (titanium) oxide system is discussed in this article.

Introduction

The spinel solid solution $Li_yTi_{2-y}O_4$ ($0 \le y \le 1/3$), which was first reported by Deschanvres et al.,[1] is a well-known anode electrode material for Li ion secondary batteries.[2−4] These materials undergo reversible lithium insertion/removal up to composition $x = 1$ in $Li_xLi_yTi_{2-y}O_4$ without significant changes in cell volume (less than 2%) and show good capacity retention. In addition, much attention has been paid to the composition of $LiTi_2O_4$, which was the first discovered superconducting oxide system having $T_C > 10$ K.[5] For this reason, numerous studies have been carried out on the electronic structure of the lithium titanate oxides with spinel structure.[6−11] However, few reports exist that describe the electronic structural changes of the lithium titanium oxides upon electrochemical Li insertions. Part of the reason is the experimental difficulty that special attention is needed because electrochemically prepared samples easily react with moisture in the air.

Conventionally, lithium insertion into transition metal (TM) oxides has been denoted by d-electron exchange in TM levels due to the various oxidation states of TM elements, which make it possible to maintain electrical neutrality by obtaining higher or lower oxidation states when Li is inserted and/or removed. For instance, the electrochemical Li insertion in $LiTi_2O_4$ spinel can be expressed by

$$Li^+ + e^- + Li^+Ti_2^{3.5+}O_4^{2-} \rightarrow Li_2^+Ti_2^{3+}O_4^{2-} \qquad (1)$$

However, recent theoretical and experimental reports have pointed out the significant role of oxide ions, which participate in the electronic exchange process upon lithium insertion reactions.[12−19] These concepts basically depend on the fact that the TM d−O 2p hybridized orbitals formed around the Fermi energy (E_F) level in which the electron exchange process occurred; therefore, electronic structural changes have to occur around oxide ions as well as TM ions.

In view of orbital hybridization, it has been generally known that early 3d TM oxides (such as Ti and V) have been described to show less hybridization between TM 3d and O 2p orbitals, because of the relatively large energy gap between TM 3d and O 2p orbitals compared with late 3d TM oxides (such as Co and Ni).[20] Accordingly, small changes in electronic structure around oxide ions are expected in the early 3d TM oxides during the electron exchange process. However, several groups have argued that the hybridization between O 2p and TM 3d orbitals would not be completely negligible even in early 3d TM compounds.[11,21−26] These topics motivated the need to investigate the role of oxide ions in electronic structural changes in this early 3d TM oxide system.

In this paper, we tried to describe the electronic structural changes of lithium titanate spinel oxide accompanied by electrochemical lithium insertions by the combination of X-ray absorption spectroscopy (XAS) experiments and first principles calculations.

Structural Description

The crystal structure of the spinel oxide $LiTi_2O_4$ has been reported by several researchers.[27−29] The spinel structure is cubic (space group $Fd\bar{3}m$) with eight AB_2X_4 units per unit cell, in which lithium ions locate at 8a tetrahedral sites, titanium ions at 16d octahedral sites, and oxide ions at 32e sites, respectively (Figure 1a). During electrochemical reactions, newly inserted lithium ions locate in empty 16c octahedral sites, while lithium ions that already exist at 8a tetrahedral sites shift to 16c octahedral sites due to repulsive forces against lithium ions at 16c sites, causing phase transformation from spinel structure to cation ordered rock salt type structure (Figure 1b).[30,31]

Experimental Section

$LiTi_2O_4$ was synthesized by conventional solid-state reactions. Li_2CO_3 and TiO_2 (Soekawa Chemicals Industries, Ltd.) were ground stoichiometrically and heated at 750 °C under an oxygen environment for 2 h. The obtained compound and titanium metal powder were thereafter mixed and pelletized. The pellets were sealed in a silica tube under vacuum conditions. The pellets were heated to 850 °C for 48 h. The electrochemical reaction of Li insertion was performed utilizing a three-electrode cell under inert gas (Ar) conditions. The working electrodes were made by mixing active material ($LiTi_2O_4$), polytetraflouroethylene (PTFE) binder, and Acetylene black (80:10:10 wt %)

* Corresponding author. E-mail: mwakihar@o.cc.titech.ac.jp.

10.1021/jp040499+ CCC: $30.25
Published on Web 12/01/2004

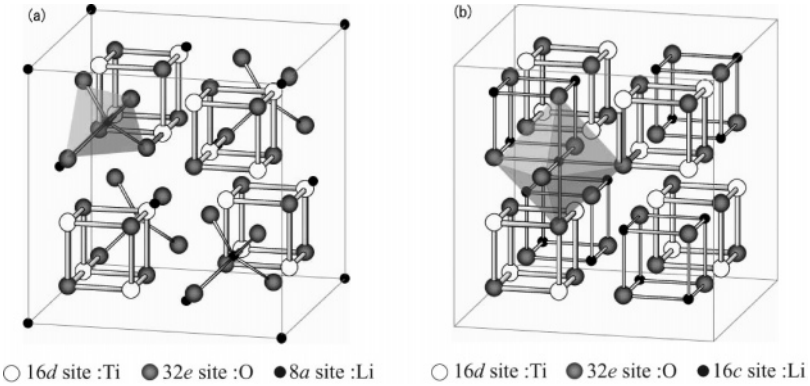

Figure 1. Schematic figure of (a) spinel structure and (b) cation ordered rock salt type structure.

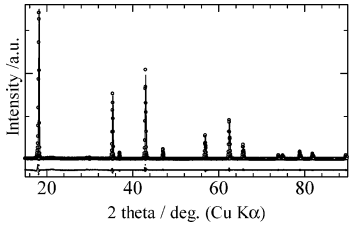

Figure 2. Observed (dot) and calculated (line) Rietveld refinement patterns of $LiTi_2O_4$. The difference between observed and calculated profiles is plotted below.

as a current collector. Li foil (Aldrich) was used as counter electrode and reference electrode. The electrolyte used was 1 M solution of $LiClO_4$ in anhydrous propylene carbonate (PC, Tomiyama's High Purity Chemicals).

X-ray diffraction measurement was carried out by using a Rigaku RINT2500V diffractometer with Cu Kα ($\lambda = 1.5418$ Å) radiation for phase identification and structural characterization.

XAS for Ti K-edge spectra was performed in transmission mode at the Photon Factory BL-7C beamline (High Energy Accelerator Research Organization, Tsukuba, Japan). The absorption peak of Cu K-edge was used for calibration of the absolute energy scale. XAS for O K-edge spectra were measured by utilizing synchrotron radiation at UVSOR BL-8B1 beamline (Institute of Molecular Science, Okazaki, Japan). The scale of absorption was determined by the total-electron-yield method. The total yield was divided by the storage-ring current which was recorded simultaneously. The absolute energy scale was determined against the standard material, TiO_2 (anatase).[32] The experiments were all performed under inert gas circumstances in order to not expose electrochemically reacted samples to air.

Results and Discussion

Figure 2 presents the observed and calculated Rietveld analysis of X-ray diffraction data for the parent powder of spinel $LiTi_2O_4$. The refined parameters are tabulated in Table 1. The site occupancies of all the ions were fixed at 1. The value of the Debye−Waller coefficient B in the 8a sites (Li) was fixed as $B = 1$ because of the low scattering ability of lithium ion, which is supported by previous neutron diffraction studies.[34] Structure refinement of $LiTi_2O_4$ by Rietveld analysis indicates that a single-phase spinel crystal structure is obtained and reveals that Li and Ti ions are distributed at tetrahedral (8a) and octahedral (16d) sites, respectively. The results are in good agreement with previous X-ray and neutron diffraction reports.[27−30] The validity of the Rietveld analysis is supported by the small refinement quality parameters R_{wp}, R_p, and S listed in Table 1. These refined data were used as the initial structural parameters for first principles calculations shown below.

TABLE 1: Structural Parameters of $LiTi_2O_4$ Obtained by Rietveld Analysis of the X-ray Diffraction Data*

space group: $Fd\bar{3}m$ (No. 227)
lattice parameters: $a = b = c = 8.4029$ (2) Å, $\alpha = \beta = \gamma = 90°$
$R_{wp} = 12.05\%$, $R_p = 8.06\%$, $S = 1.6235$

atom	site	x (=y = z)	B (Å^2)
Li	8a	0	1
Ti	16d	0.625	0.86 (3)
O	32e	0.3890 (1)	0.30 (5)

[a] Each refinement quality parameter is defined as follows: $R_{wp} = [\sum_i w(y_{i,obs} - y_{i,calc})^2/\sum_i w_i y_{i,obs}]^{1/2}$; $R_p = \sum_i |y_i - f_i(x)|/\sum_i y_i$; $S = R_{wp}/R_p$.

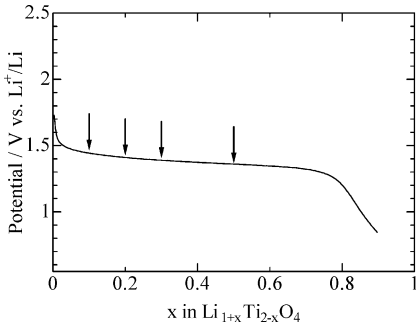

Figure 3. Variation of cell voltage with electrochemical insertions (current density 20 μA/cm^2). The arrows indicate the samples for the XAS measurement.

We have performed experiments showing the variation of the cell potential through electrochemical lithium insertion under low galvanostatic current (20 μA/cm^2) in Figure 3. The arrows in the figure show the samples for XRD and XAS measurements. The relatively flat potential plateau, observed around 1.38 V in the whole range of the Li insertion process, might relate to the two-phase coexistence mechanism of the reaction suggested previously.[2,4]

X-ray diffraction powder patterns of $Li_{1+x}Ti_2O_4$ ($0 \le x \le 0.5$) in Figure 4, obtained by electrochemical Li insertions at room temperature, do not show any noticeable changes. This result suggests that the host structure which titanium and oxide ions build remains unchanged during electrochemical Li insertions.

The Ti K-edge XAS spectra of $Li_{1+x}Ti_2O_4$ ($0 \le x \le 0.5$) represent the transition from Ti 1s orbitals to the unoccupied p orbitals (Figure 5). XAS in this energy area reflect electronic structures such as oxidation states of absorbing atoms. Figure 5 indicates that XAS gradually shifts to lower energy along with increasing amount of electrochemical lithium insertions. Con-

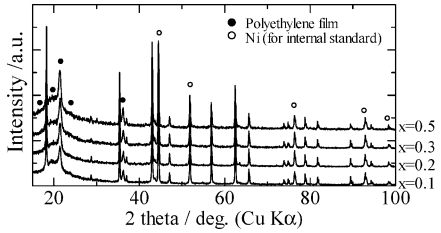

Figure 4. Powder X-ray diffraction patterns of the spinel compounds $Li_{1+x}Ti_2O_4$ obtained by electrochemical Li insertion.

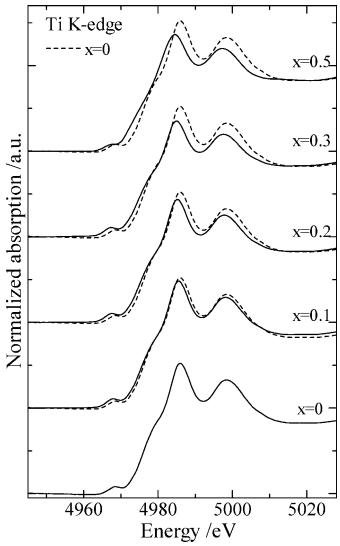

Figure 5. Ti K-edge XAS spectra of $Li_{1+x}Ti_2O_4$ ($0 \le x \le 0.5$).

sequently, it was confirmed that the reduction process of titanium ion developed during electrochemical lithium insertions as shown in eq 1.

The O K-edge XAS spectra of $Li_{1+x}Ti_2O_4$ ($0 \le x \le 0.5$) in Figure 6a show that the transitions from the O 1s core level to the unoccupied 2p level emerge due to the dipole transition selection rules. The peak intensity in O K-edge XAS is linearly related to the number of unoccupied holes in oxygen p orbitals, which means that covalency should be considered (note that the electronic configuration of the complete ionic O^{2-} model is $[He]2s^22p^6$, which has no unoccupied p orbital hole). The two sharp peaks A and B, which were observed at lower energy up to 535 eV in Figure 6a, are assigned to the transitions from O 1s orbital to the hybridized orbital between O 2p and Ti 3d levels. The electrons in d orbitals are likely to localize, so the width of the peak becomes sharp. Also, the broad peaks at higher energy above 535 eV show the transition from O 1s to the hybridized orbital between O 2p and Ti 4sp levels.[32,33] In addition, peaks A and B at lower energy region, which are attributed to the O 2p hybridized orbital with Ti 3d t_{2g} and e_g orbitals split by crystal field theory, are roughly 3 eV apart. This energy gap in O K-edge XAS is consistent with the results of first principles calculations shown below. The intensity of peak A near 530 eV gradually decreases along with the increasing amount of electrochemically inserted lithium ions (see Figure 6b, the area ratio of peaks A and B which was obtained by fitting the Gaussian function). In other words, the transition probability to unoccupied O 2p orbitals (the number of holes) diminished as Li ion insertion proceeds. Accordingly, O K-edge XAS results revealed that the oxide ions also contribute to the electron exchange reactions upon electrochemical lithium insertion, even though it was conventionally considered that the early 3d TM oxides do not form large TM 3d and O 2p hybridized orbitals.

To verify our interpretation of experimental XAS, first principles calculations were performed using Wien2k program code based on linearized augmented plane wave + local orbital (LAPW+lo).[35] The generalized gradient approximation was applied by using Perdue's algorithm.[36] The number of *k* points in the whole Brillouin zone was set to be $10 \times 10 \times 10$ during the self-consistent iterations. The lithium titanate spinel oxide $LiTi_2O_4$ and lithium-inserted $Li_2Ti_2O_4$ unit models, employed under cubic symmetry (space group $Fd\bar{3}m$), were calculated to investigate the electronic structural changes. The structural parameter obtained by Rietveld analysis of $LiTi_2O_4$ (see Table 1) was used for the first principles calculation of $LiTi_2O_4$. In the $Li_2Ti_2O_4$ unit model, all Li ions fully locate at 16c octahedral sites within the same Ti_2O_4 host structure. Both unit models are calculated under the constraint of constant volume, because there is only a slight change in lattice parameters during electrochemical Li ion insertions on $LiTi_2O_4$ spinel[2−4] as mentioned in the Introduction.

Figure 7 displays total and local orbital-projected density of states (DOS) of $LiTi_2O_4$ (before Li insertion) and $Li_2Ti_2O_4$ (after Li insertion) obtained by first principles calculations. The Fermi energy was set as 0 eV in the energy scale. As shown in the Figure 7, there are three electronic states—bands a, b, and c—around the Fermi energy region in the total DOS of both $LiTi_2O_4$ and $Li_2Ti_2O_4$. Ti d and O p local DOS showed that the valence band (band a) and the conduction band (bands band c) were mainly composed of O 2p orbital and Ti 3d orbital, respectively.

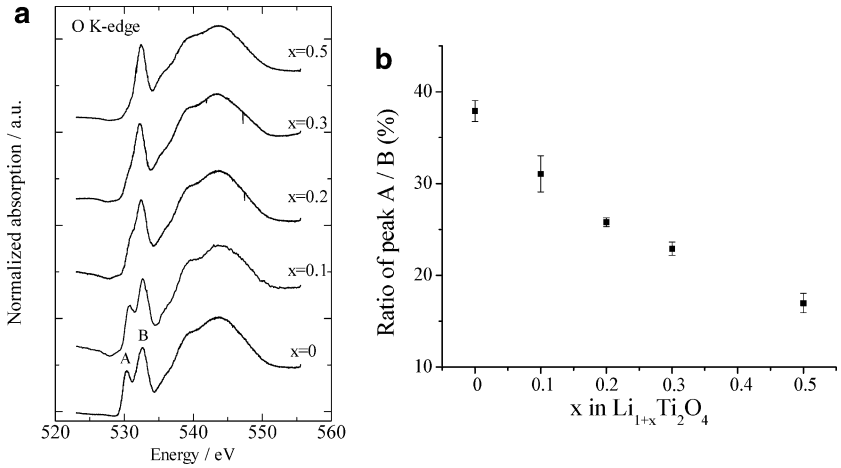

Figure 6. (a) O K-edge XAS spectra of $Li_{1+x}Ti_2O_4$ ($0 \le x \le 0.5$). (b) Gaussian fitting of the ratio of peaks A and B of O K-edge XAS spectra of $Li_{1+x}Ti_2O_4$ ($0 \le x \le 0.5$).

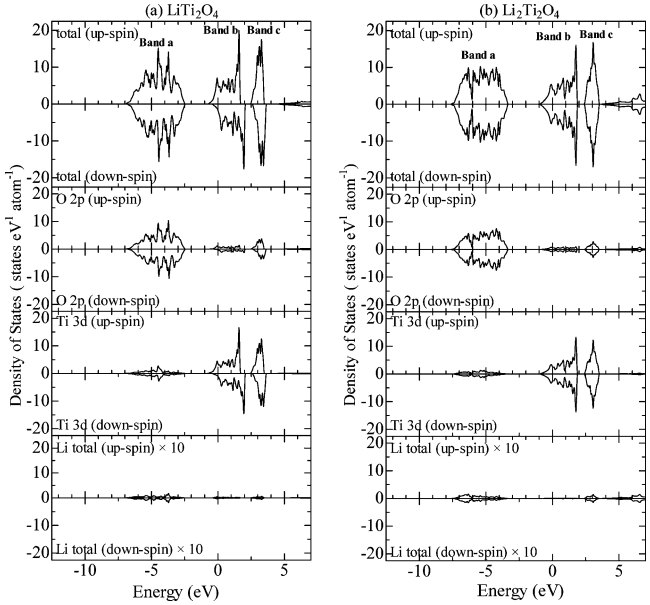

Figure 7. Total and partial density of states (DOS) of (a) $LiTi_2O_4$ (before Li insertion) and (b) $Li_2Ti_2O_4$ (after Li insertion).

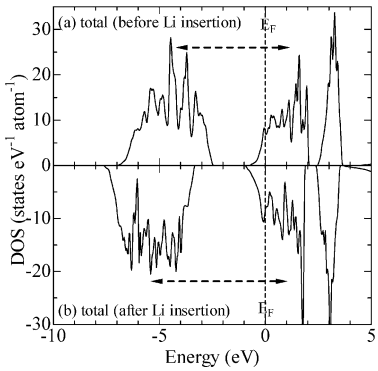

Figure 8. Comparison between total densities of states (DOS) of (a) $LiTi_2O_4$ (before Li insertion) and (b) $Li_2Ti_2O_4$ (after Li insertion).

Furthermore, the local DOS of Li (for a clear view, DOS is 10 times as large as the real value) is apart from the Fermi energy level, and little relationships between Ti and O orbital were indicated. As a result, it is possible to speculate that the Li ions are strongly ionized in both the $LiTi_2O_4$ and $Li_2Ti_2O_4$ structures. On the other hand, local DOS figures evidently show that Ti 3d and O 2p levels form a hybridized orbital near the Fermi energy. Specifically, Ti 3d bands are split into 3-fold degenerate t_{2g} (nonbonding, dp_π)-like and 2-fold degenerate e_g (antibonding, dp_σ)-like bands, showing that Ti ions are under octahedral configuration. Therefore, the two peaks A and B shown in O K-edge XAS (Figure 6a) are attributed to the hybridized orbital of Ti t_{2g} and e_g states (bands b and c), respectively. The calculated energy separation (~3 eV) between t_{2g} and e_g states in Figure 7 are consistent with the experimental one (Figure 6a). The decreasing intensity of peak A in O K-edge XAS indicates that the increased number of electrons due to the electrochemically doping Li ion occupied Ti t_{2g}−O 2p hybridized orbital, confirming that the oxide ions also contribute to the charge compensation process during electrochemical reactions.

Furthermore, the energy gap between valence band and conduction band gets broader by lithium ion insertions (Figure 8), suggesting the covalent characters between O 2p and Ti 3d orbitals decreased. Hence, the charge compensation around oxide ions mentioned above could be described in the following way: the increments of the ionicity induced by the lithium insertion and the reduction process of Ti ions cause the redistribution of electrons in the system, and then oxide ion partly receives the electrons to enhance the negative ionic (anionic) characters.

Two-dimensional electron densities and their differences between the two unit models ($\rho(LiTi_2O_4) - \rho(Li_2Ti_2O_4)$) are presented in Figures 9 and 10 based on the results of first principles calculations to confirm the discussions mentioned above. There exists strong covalent bonding between Ti and oxide ions (Figure 9), while electrons around Li ion are isolated from O 2p orbital, or Li ion strongly ionized in this structure. This indication is in accordance with the discussions above in the local DOS of each ion (Figure 7). In Figure 10, white and black regions show positive and negative electron density differences, respectively. Li ions at 8a site and 16c site show the occupied location of the two unit models, before and after Li insertions. First, the titanium ion site is the densest black area (area 1) for electron transfer changes, which stressed active compensation by Ti ions for electron density changes due to Li ion insertions. Oxide ion central sites (area 2) show rather small, but dense electron density increases. These combined results imply that the oxide ions as well as Ti ions contribute to the charge compensation for the electrochemical Li insertion. From this perspective, the study of lithium intercalation on TiO_2 by Koudriachova et al.[37,38] also supports our experimental and computational conclusions, since they showed that approximately half of the additional electron is transferred to the Ti ions and 25%−30% to the O ions from the computational results based on density functional theory. Second, more positive values (decrease in electron density) than its surroundings were observed at the area between Ti and oxide ions (area 3), indicating the area in which the Ti−O covalent bond is developed. These electron density changes support the reduction process of Ti ions leading up to the increasing ionicity in this

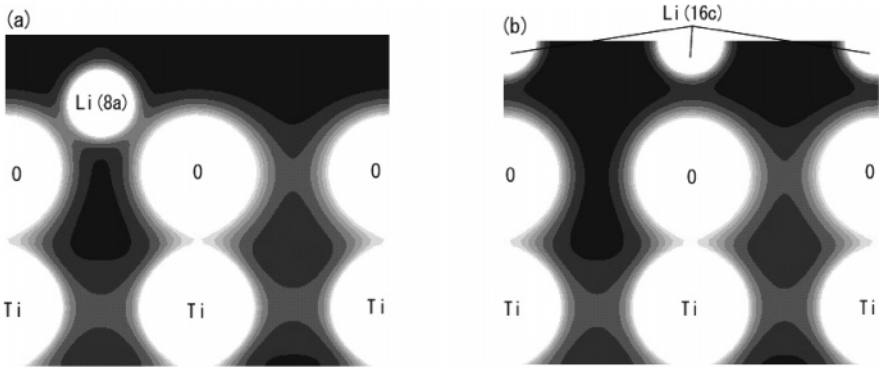

Figure 9. Calculated charge density of (110) plane for (a) $LiTi_2O_4$ (before Li insertion) and (b) $Li_2Ti_2O_4$ (after Li insertion).

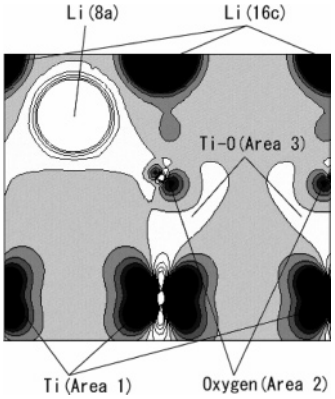

Figure 10. Calculated charge density differences between $LiTi_2O_4$ and $Li_2Ti_2O_4$ within the (110) plane by the first principles calculation method. White regions show positive electron density differences, while black regions indicate negative electron density differences.

system, which causes electron redistribution especially around Ti and oxide ions. Accordingly, the charge compensation around oxide ions as well as Ti ions can be attributed to the increase of ionicity induced by the reduction process of Ti ions upon electrochemical Li ion insertions.

Conclusions

Electronic structural changes of electrochemically reacted lithium titanate spinel, $LiTi_2O_4$, were studied by X-ray absorption spectroscopy (XAS) measurement and first principles calculations. O K-edge XAS, along with electrochemical Li ion insertions, show the changes in peak intensity that represent the transition from O 1s to hybridized O 2p−Ti 3d (t_{2g}) states. Furthermore, density of states and electron density differences based on first principles calculations imply that enhanced ionicity between oxide ions and Ti ions, induced by the reduction process of Ti ions upon Li insertions, causes electronic structural changes in the system. As a result, this suggests the considerable effect of oxide ions for the charge compensation process in this early 3d TM oxide.

Acknowledgment. This work was supported by a Grant-in-Aid for Scientific Research on Priority Areas (B) (No.740) "Fundamental Studies for Fabrication of All Solid State Ionic Devices" from Ministry of Education, Culture, Sports, Science and Technology, Japan. The Ti K-edge XAS experiments were performed at the PF with the approval of the High Energy Accelerator Research Organization (Proposal No.2002G254), and O K-edge XAS measurements were executed at UVSOR with the approval of the Institute for Molecular Science (Proposal No.13-876).

References and Notes

(1) Deschanvres, A.; Raveau, B.; Sekkal, Z. *Mater. Res. Bull.* **1971**, *6*, 64.
(2) Colbow, K. M.; Dahn, J. R.; Haering, R. R. *J. Power Sources* **1989**, *26*, 397.
(3) Ferg, E.; Gummow, R. J.; de Kock, A.; Thackeray, M. M. *J. Electrochem. Soc.* **1994**, *141*, L147.
(4) Ohzuku, T.; Ueda, A.; Yamamoto, N. *J. Electrochem. Soc.* **1995**, *142*, 1431.
(5) Johnston, D. C.; Prakash, H.; Zachariasen, W. H.; Viswanathan, R. *Mater. Res. Bull.* **1973**, *8*, 777.
(6) Edwards, P. P.; Egdell, R. G.; Fragala, I.; Goodenough, J. B.; Harrison, M. R.; Orchard, A. F.; Scott, E. G. *J. Solid State Chem.* **1984**, *54*, 127.
(7) Satpathy, S.; Martin, R. M. *Phys. Rev. B* **1987**, *36*, 7269.
(8) Massidda, S.; Yu, J.; Freeman, A. J. *Phys. Rev. B* **1988**, *38*, 11352.
(9) Oda, T.; Shirai, M.; Suzuki, N.; Motizuki, K. *Physica B* **1996**, *219*−*220*, 451.
(10) Takahashi, Y.; Gotoh, Y.; Akimoto, J. *J. Phys. Chem. Solids* **2002**, *63*, 987.
(11) Ra, W.; Nakayama, M.; Ikuta, H.; Uchimoto, Y.; Wakihara, M. *Appl. Phys. Lett.* **2004**, *84*, 4364.
(12) Aydinol, M. K.; Kohan, A. F.; Ceder, G.; Cho, K.; Joannopoulos, J. *Phys. Rev. B* **1997**, *56*, 1354.
(13) Ceder, G.; Chiang, Y.-M.; Sadoway, D. R.; Aydinol, M. K.; Jang, Y.-I.; Huang, B. *Nature* **1998**, *392*, 694.
(14) Ceder, G. *Science* **1998**, *280*, 1099.
(15) Benco, L.; Barras, J.-L.; Atanasov, M.; Daul, C. A.; Deiss, E. *Solid State Ionics* **1998**, *112*, 255.
(16) Berg, H.; Göransson, K.; Noläng, B.; Thomas, J. O. *J. Mater. Chem.* **1999**, *9*, 2813.
(17) Uchimoto, Y.; Sawada, H.; Yao, T. *J. Power Sources* **2001**, *97*−*98*, 326.
(18) Graetz, J.; Ahn, C. C.; Yazami, R.; Fultz, B. *J. Phys. Chem. B* **2003**, *107*, 2887.
(19) Nakayama, M.; Imaki, K.; Ra, W.; Ikuta, H.; Uchimoto, Y.; Wakihara, M. *Chem. Mater.* **2003**, *15*, 1728.
(20) Zaanen, J.; Sawatzky, G. A.; Allen, J. W. *Phys. Rev. Lett.* **1985**, *55*, 418.
(21) Uozumi, T.; Okada, K.; Kotani, A. *J. Phys. Soc. Jpn.* **1993**, *62*, 2595.
(22) Parlebas, J. C.; Khan, M. A.; Uozumi, T.; Okada, K.; Kotani, A. *J. Electron Spectrosc. Relat. Phenom.* **1995**, *71*, 117.
(23) Uozumi, T.; Okada, K.; Kotani, A.; Zimmermann, R.; Steiner, P.; Hüfner, S.; Tezuka, Y.; Shin, S. *J. Electron Spectrosc. Relat. Phenom.* **1997**, *83*, 9.
(24) Zimmermann, R.; Claessen, R.; Reinert, F.; Steiner, P.; Hüfner, S. *J. Phys.: Condens. Matter* **1998**, *10***,** 5697.
(25) Fujimori, A.; Yoshida, T.; Okazaki, K.; Tsujioka, T.; Kobayashi, K.; Mizokawa, T.; Onoda, M.; Katsufuji, T.; Taguchi, Y.; Tokura, Y. *J. Electron Spectrosc. Relat. Phenom.* **2001**, *117*−*118*, 227.
(26) Bocquet, A. E.; Mizokawa, T.; Morikawa, K.; Fujimori, A.; Barman, S. R.; Maiti, K.; Sarma, D. D.; Tokura, Y.; Onoda, M. *Phys. Rev. B* **1996**, *53***,** 1161.
(27) Johnston, D. C. *J. Low Temp. Phys.* **1976**, *25*, 145.
(28) Dalton, M.; Gameson, I.; Armstrong, A. R.; Edwards, P. P. *Physica C* **1994**, *221***,** 149.
(29) Green, M. A.; Dalton, M.; Prassides, K.; Day, P.; Neumann, D. A. *J. Phys.: Condens. Matter* **1997**, *9***,** 10855.
(30) Cava, R. J.; Murphy, D. W.; Zahurak, S.; Santoro, A.; Roth, R. S. *J. Solid State Chem.* **1984**, *53*, 64.
(31) Zachau-Christiansen, B.; West, K.; Jacobsen, T.; Atlung, S. *Solid State Ionics* **1990**, *40*−*41*, 580.
(32) de Groot, F. M. F.; Grioni, M.; Fuggle, J. C.; Ghijsen, J.; Sawatzky, G. A.; Peterson, H. *Phys. Rev. B* **1989**, *40*, 5715.
(33) Soriano, L.; Abbate, M.; Fuggle, J. C.; Jimeénez, M. A.; Sanz, J. M.; Mythen, C.; Padmore, H. A. *Solid State Commun.* **1993**, *87*, 699.
(34) Oikawa, K.; Kamiyama, T.; Izumi, F.; Nakazato, D.; Ikuta, H.; Wakihara, M. *J. Solid State Chem.* **1999**, *146*, 322.
(35) Blaha, P.; Schwarz, K.; Madsen, G. K. H.; Kvasnicka D.; Luitz, J. *WIEN2k, An Augmented plane Wave + Local Orbitals Program for Calculating Crystal Properties*; Karlheinz Schwarz, Technisches Universität Wien: Vienna, Austria, 2001.
(36) Perdew, J. P.; Burke, K.; Ernzerhof, M. *Phys. Rev. Lett.* **1996**, *77*, 3865.
(37) Koudriachova, M. V.; Harrison, N. M.; Leeuw, S. W. *Phys. Rev. B* **2004**, *69*, 054106.
(38) Koudriachova, M. V.; Leeuw, S. W. *Phys Rev. B* **2002**, *65*, 235423.